AGU ADVANCING EARTH AND SPACE SCIENCE

Water Resources Research

RESEARCH ARTICLE
10.1029/2020WR028789

Influence of Invasive Submerged Aquatic Vegetation (*E. densa*) on Currents and Sediment Transport in a Freshwater Tidal System

Jessica R. Lacy[1], Madeline R. Foster-Martinez[2], Rachel M. Allen[1,3], and Judith Z. Drexler[4]

[1]U.S. Geological Survey, Pacific Coastal and Marine Science Center, Santa Cruz, CA, USA, [2]University of New Orleans, Pontchartrain Institute for Environmental Sciences, New Orleans, LA, USA, [3]Department of Civil and Environmental Engineering, University of California, Berkeley, CA, USA, [4]U.S. Geological Survey, California Water Science Center, Sacramento, CA, USA

Key Points:

- In dense patches of *E. densa* at two sites, the vegetation frontal area was similar and currents were attenuated by more than 90%
- Tidally averaged suspended-sediment concentration (SSC) depletion within the vegetation was approximately 20% at one site and 0–40% at a second site
- Submerged aquatic vegetation (SAV) fringing channels reduces sediment delivery to marshes by 20%–30%, as suspended sediment deposits in the SAV before reaching the marsh

Correspondence to:
J. R. Lacy,
jlacy@usgs.gov

Citation:
Lacy, J. R., Foster-Martinez, M. R., Allen, R. M., & Drexler, J. Z. (2021). Influence of invasive submerged aquatic vegetation (*E. densa*) on currents and sediment transport in a freshwater tidal system. *Water Resources Research*, *57*, e2020WR028789. https://doi.org/10.1029/2020WR028789

Received 9 SEP 2020
Accepted 26 JUN 2021

Abstract We present a field study combining measurements of vegetation density, vegetative drag, and reduction of suspended-sediment concentration (SSC) within patches of the invasive submerged aquatic plant *Egeria densa*. Our study was motivated by concern that sediment trapping by *E. densa*, which has proliferated in the Sacramento–San Joaquin Delta, is impacting marsh accretion and reducing turbidity. In the freshwater tidal Delta, *E. densa* occupies shallow regions frequently along channel margins. We investigated two sites: Lindsey Slough, a muddy low-energy backwater, and the lower Mokelumne River, with stronger currents and sandy bed sediments. At the two sites, biomass density, frontal area, and areal density of the submerged aquatic vegetation (SAV) were similar. Current attenuation within *E. densa* exceeded 90% and the vegetative drag coefficient followed $C_d = 174 Re_d^{-1.46}$, where Re_d is stem Reynolds number. The SAV reduced SSC by an average of 18% in Lindsey Slough. At the Mokelumne River the reduction ranged 0%–40%, with greatest trapping when discharge and SSC were elevated. This depletion of SSC decreases the transport of sediment to marshes by the same percentage, as the rising tide must pass through fringing SAV before reaching marshes. Sediment trapping in *E. densa* in the Delta is limited by low flux through the canopy and low settling velocity of suspended sediment (mostly flocculated mud). Sediment trapping by SAV has the potential to reduce channel SSC, but the magnitude and sign of the effect can vary with local factors including vegetative coverage and the depositional or erosional nature of the setting.

1. Introduction

In rivers, estuaries, and coastal waters, the drag exerted by submerged aquatic vegetation (SAV) reduces water velocity, which promotes settling and trapping of suspended sediment (Madsen et al., 2001). Slower currents, lower turbidity, and accretion are beneficial to SAV, and SAV can benefit ecosystems. However, when the SAV is dense, which is typical of invasive aquatic vegetation (IAV), these alterations to the physical environment tend to have negative effects on ecosystems and to impede human uses of waterways by reducing conveyance and obstructing navigation (Santos et al., 2011).

In recent decades, both floating and submerged IAV have proliferated in the Sacramento–San Joaquin Delta (Delta), joining a myriad of invasive species over a broad range of taxa that have become established in the San Francisco Bay and Delta (Cohen & Carlton, 1998). The perennial freshwater submerged macrophyte *Egeria densa*, a native of South America that has spread around the world, was widespread in the Delta by the 1990s (Yarrow et al., 2009). It is now the most abundant submerged plant in the region, inhabiting channel margins and restored subtidal shallows in former agricultural tracts; efforts to eradicate or control *E. densa* are ongoing but have limited effectiveness (Santos et al., 2011; Durand et al., 2016). The impacts of *E. densa* on the Delta ecosystem include displacing native SAV, altering the water quality, and harboring predatory non-native fishes (Nobriga et al., 2005; Santos et al., 2011). *E. densa* also affects currents and sediment transport, which is the topic of this paper.

The influence of submerged vegetation on hydrodynamics is well understood as a result of laboratory studies. Two hydrodynamic zones have been identified in SAV (Nepf & Vivoni, 2000). The vertical exchange

zone is at the top of the canopy, where turbulence generated at the canopy–water interface extends into the vegetation down to the penetration height h_p, mixing momentum as well as dissolved and suspended matter between the canopy and the water above. Below h_p is the longitudinal exchange zone, in which the turbulence is dominated by stem wakes and exchange with the surrounding water occurs through advection.

Current damping within SAV has been observed in many field studies in both marine and fresh waters, as summarized by Jones et al. (2012). However, in most of these studies, the data are too limited to be interpreted using the theoretical framework provided by laboratory studies or to quantify attenuation. Measurements of vegetation density or frontal area are frequently lacking. There are far fewer field studies on the influence of SAV on suspended-sediment concentration (SSC) and sediment transport (Gurbisz et al., 2016; Hansen & Reidenbach, 2013; Work et al., 2020). Among field studies of currents and sediment transport in SAV, our study of *E. densa* is unusual because the vegetation is very dense and often occupies the full water depth. In the Delta, *E. densa* primarily occupies bed elevations from 1 m above to 2 m below mean lower low water (MLLW), and extends across the entire water column for most of the tidal cycle (Durand et al., 2016). As a result, the longitudinal exchange zone extends over the full canopy, except at high tide or during high river flows.

In this paper, we present measurements of vegetation density and current velocity, SSC, and bed sediment grain size distribution within and outside patches of *E. densa*, at two sites in the Sacramento–San Joaquin Delta. We determine rates of current attenuation, vegetative drag, and suspended-sediment depletion by *E. densa*, providing results that can be used in numerical modeling of large-scale effects of *E. densa* in the Delta and other systems inhabited by dense SAV. We address differences in the mechanisms and magnitude of sediment trapping related to the hydrodynamic settings of the two study sites and consider the implications of the patch-scale effects for SSC and suspended-sediment flux in the Delta and for sediment delivery to Delta marshes. The latter is of particular concern because accelerating sea level rise is increasing the need for marsh sediment accretion (Swanson et al., 2015), whereas sediment yield and turbidity in the Delta have decreased by approximately 50% in the past 50 years (Wright & Schoellhamer, 2004; Work et al., 2020). This work is part of a larger study on sediment trapping in SAV in the Delta. In companion papers, Work et al. (2020) report results from an alternate method of estimating sediment trapping in SAV, and Drexler et al. (2021) present rates of sediment and organic carbon accumulation determined from cores collected in the SAV and marshes at our study sites.

2. Methods

2.1. Study Sites

We conducted the study in the Sacramento–San Joaquin Delta, an extensive tidal, freshwater region at the landward end of the San Francisco Estuary (Figure 1). The Delta hosts a highly productive ecosystem and also serves as a source of fresh water for much of California, forming a critical link in one of the largest water delivery systems in the world (Luoma et al., 2015). Humans have modified the Delta for navigation, water conveyance, and agriculture. Habitat loss, water diversion, contaminants, and invasive species have impacted the Delta ecosystem, and the populations of native fishes have plummeted (Nichols et al., 1986; Sommer et al., 2007). These impacts are now exacerbated by a changing climate and rising sea level (Luoma et al., 2015). Most of the once-extensive marsh in the Delta was drained for agriculture in the late nineteenth and early twentieth centuries (Nichols et al., 1986). Today, it is a complex network of natural and constructed channels, levees, and shallow tidal basins. Sediment is supplied to the Delta by the Sacramento and San Joaquin rivers, mostly during high flows that occur in winter and spring (Conomos et al., 1985; Wright & Schoellhamer, 2005). Sediment delivery to the Delta is declining, most likely due to the end of hydraulic mining and the construction of reservoirs: It decreased by about 50% between 1957 and 2001 (Wright & Schoellhamer, 2004). Turbidity in the Delta declined over the same period (Hestir et al., 2016; Work et al., 2020).

Data collection focused on two sites: Lindsey Slough (LS), a tidal backwater in the Cache Slough Complex in the north Delta, and the Mokelumne River (MOK) near the confluence with the San Joaquin River in the central Delta, where riverine influence and tidal currents are stronger than in Lindsey Slough (Figure 1). At these two sites we acoustically mapped bathymetry and the edge of vegetation, collected biomass samples to

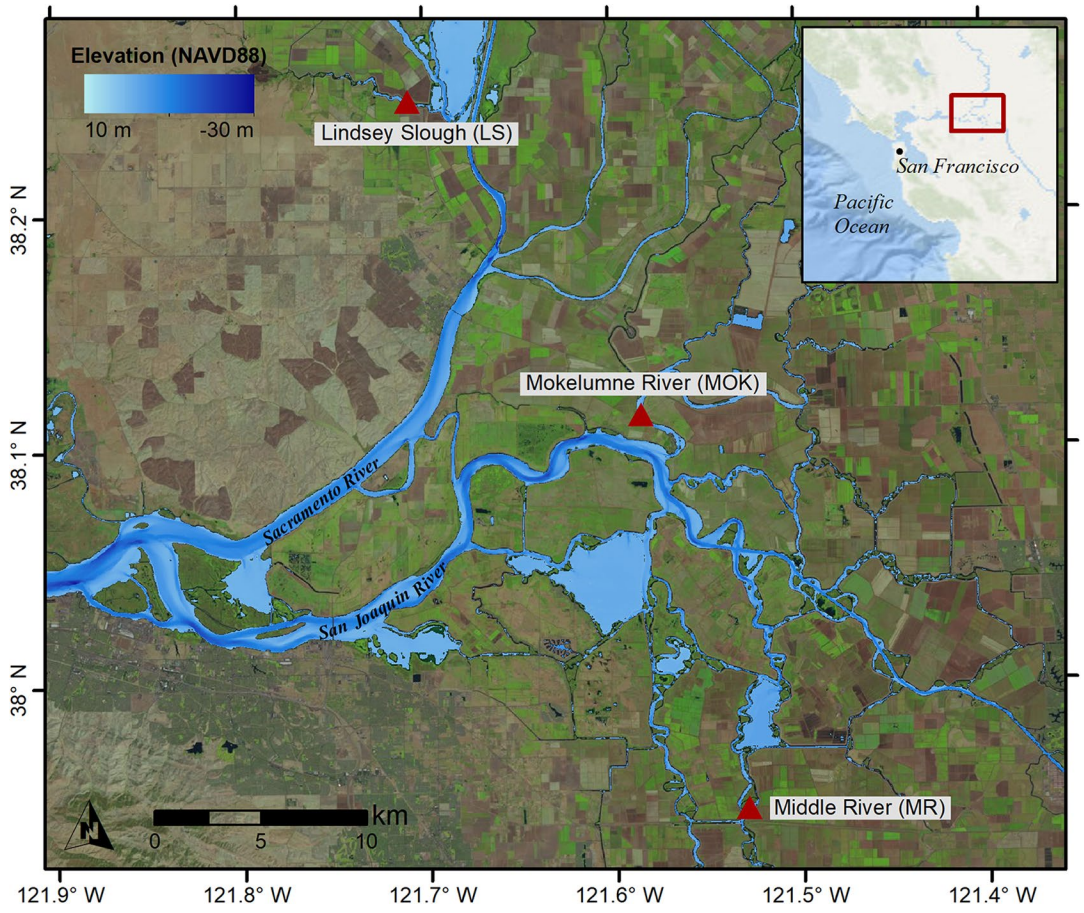

Figure 1. Map of the Sacramento–San Joaquin Delta, with locations of study sites in Lindsey Slough, Middle River, and the lower Mokelumne River. Bathymetric data from Fregoso et al. (2017); aerial imagery from Landsat 8; base map in inset tile is the intellectual property of ESRI and is used herein under license.

determine vegetation density, analyzed bed sediments, and collected time series of current velocity and SSC within and outside the vegetation patches (Figure 2). We also measured vegetation density and analyzed bed sediments from a third site, Middle River (MR). Data collection and sampling took place in LS in April 2017, and in MOK and MR in March 2018.

2.2. Vegetation Density

Divers collected SAV from 0.25 m^2 quadrats to determine density. They harvested everything rooted within the quadrat and stored it in a cloth bag for transport to the vessel. The collection was challenging because the vegetation was dense and tall, and plant branches extended beyond the quadrat area. We sampled eight quadrats in Lindsey Slough, six in the Middle River, six near the instrumented transect in the Mokelumne River (MOK-north), and four in a patch 2.7 km downstream (MOK-south) (Figure 2, MOK-south not shown). In the laboratory, quadrat samples were rinsed repeatedly with deionized water until the water ran clear. The vegetation was identified to the genus level and sorted by species. We measured the diameter at the midpoint of 20 stems or stem fragments per quadrat. Samples were dried at 40° C until they reached a constant mass (minimum of 72 h).

During the surveys, we observed that *E. densa* was the dominant species of SAV. The plants had a complex branching structure and varied widely in size, and we concluded that the typical approach of determining frontal area and areal density from stem density, number of blades per stem, and stem and blade dimensions was not practical for *E. densa*. Instead, we used photogrammetry. Divers collected individual *E. densa* plants

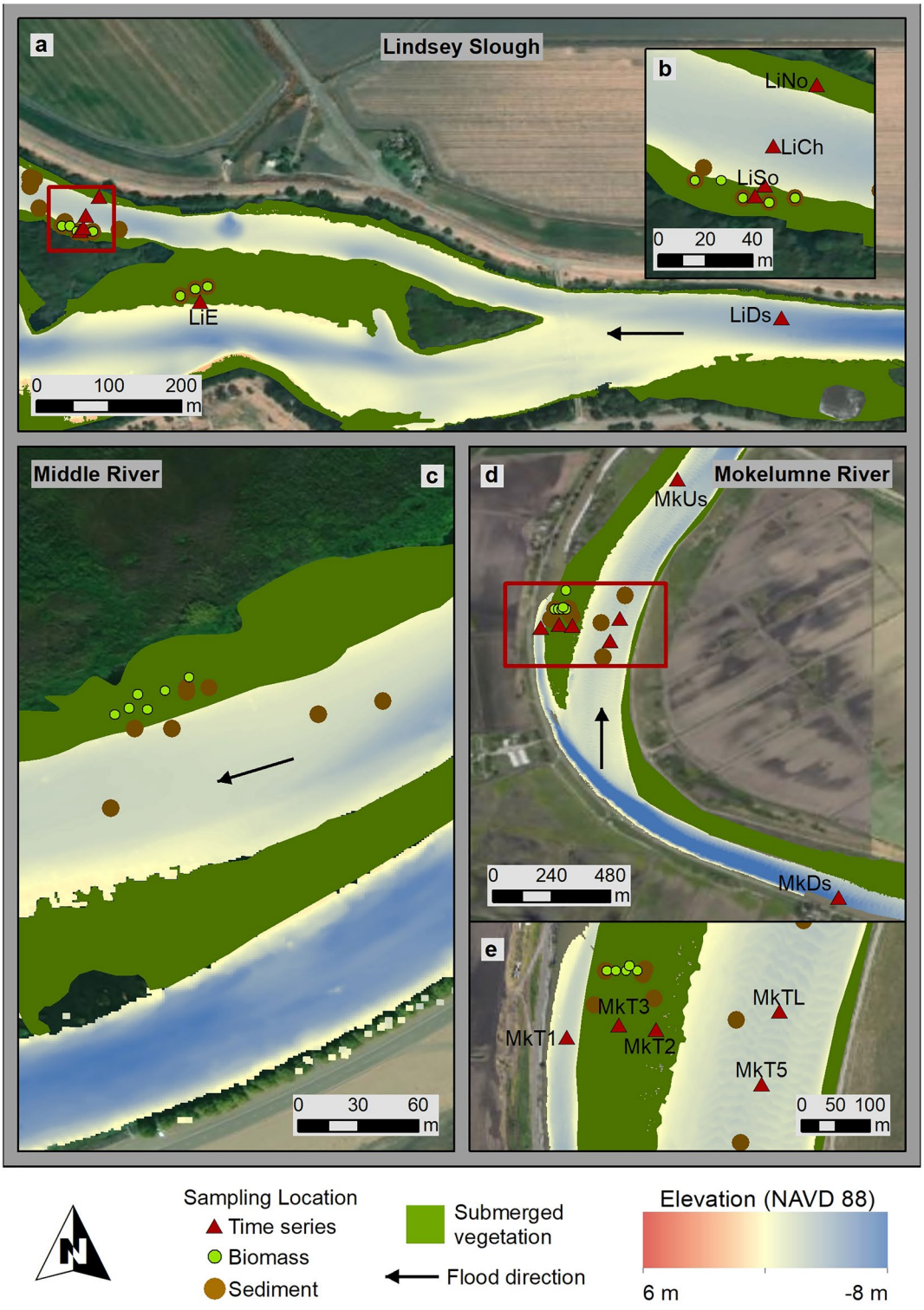

Figure 2. Maps of the study sites showing bathymetry of channels and extent of submerged aquatic vegetation, determined from acoustic backscatter, with locations of biomass samples (green circles), bed sediment samples (brown circles), time-series instrumentation (red triangles, with station IDs), and flood-tide directions (arrows). (a) Lindsey Slough, (b) Lindsey Slough detail, (c) Middle River (no time-series data collected), (d) Mokelumne River, (e) Mokelumne River detail. Bathymetry and imagery sources as in Figure 1.

for this purpose (seven from LS, six from MR and MOK-north, and four from MOK-south), keeping each one as intact as possible in a cloth bag. The intact plants were kept moist and refrigerated and were photographed within 48 h of collection. Each plant was arranged against a solid backdrop and photographed with a Nikon D810 camera mounted at a minimum distance of 2 m, using a remote trigger to minimize disturbance. Images were taken quickly before the plants shriveled (<10 min). Before and after each camera adjustment, we photographed a 1 cm checkerboard containing 10 cm squares. The plants were then dried in the same way as the quadrat samples.

We measured the dimensions of squares near the corners in each checkerboard image to use in converting pixels to area. The number of pixels per side varied by less than 2% so a distortion correction was deemed unnecessary. The images were cropped to areas containing plant material. A brightness threshold within the red channel distinguishing the plant material was determined visually for each batch of images taken with the same lighting and camera conditions. We produced binary images based on the threshold, and pixels with plant material were counted and converted to area. Measurements of stem width from the images were spot-checked against the plant measurements.

The slope m_v of plant area versus biomass was determined using the nonparametric, repeated median method (Siegel, 1982). We calculated frontal area (in m^{-1}) as $a = Bm_v / h_v$, where B is dry mass density (g / m^2) and h_v is canopy height. We did not have a direct measurement of the elevation of the canopy top, and the plant height was too variable to be used for estimating h_v. During multiple visits to both the sites, we observed that the canopy reached the water surface except at peak high tide, when the top of the vegetation was approximately 0.25 m below the water surface, which is equivalent to 0.25 m above the mean tide level (MTL) given the 1 m tide range. We estimated h_v as MTL + 0.25 m $- \overline{E}_q$, where $\overline{E}_q$ is the site-averaged bed elevation of the quadrats.

Areal density is defined as $\phi = m\pi d^2 / 4$, where m is stem density and d is stem diameter (Tanino & Nepf, 2008; Vargas-Luna et al., 2015). We expected that the leaf whorls that grow at regular intervals on *E. densa* stems would influence the areal density. To account for the whorls, we determined an effective diameter d_e from the binary images by cropping the photos to isolate 10 individual branches, measuring branch area and length, dividing the area by the length, and averaging the results. We calculated areal density as $\phi = \hat{m}\pi d_e^2 / 4$, where $\hat{m} = a / d_e$ is the equivalent stem density for cylindrical stems with no branches.

2.3. Surficial Bed Sediment Sampling and Analysis

At each site we sampled surficial bed sediments within patches and in the unvegetated channel to determine how current attenuation within the vegetation influences the properties of deposited particles. At shallow, vegetated sites we collected hand-held push cores (4.4 cm inner diameter plexiglass tubing) from a small vessel (eight in LS and five each at MOK and MR). In the channel at each site, we collected three cores with a Gomex corer (0.0625 m^2), each of which was subsampled with three push cores.

The top 1 cm of sediment from each push core was sectioned off for analysis and stored in a sealed plastic bag until weighed. To determine the bulk density, the samples were weighed wet, dried at 60°C, and weighed again. The drying was continued until the weights stabilized. The dry bulk density was calculated as BD = $(1 - P)\rho_s$, where porosity P is the fraction of water by volume and sediment density ρ_s is 2.65 g / cm^3. Both the fine fraction (< 63 μm) and the sand fraction (63 μm–2 mm) were analyzed with a laser-diffraction particle analyzer to determine the disaggregated grain size distribution.

2.4. Time-Series Data Collection

We collected time-series measurements of current velocity, water depth, and turbidity at several locations in the unvegetated channel and within patches of *E. densa* in Lindsey Slough in April 2017 and at the mouth of the Mokelumne River in March 2018. At each site we deployed a cross-channel transect of instruments from the unvegetated channel into a vegetation patch (Figure 2). In the channel, we measured velocity profiles over the bottom meter, high-frequency (8 Hz) bursts of velocity near the bed with an acoustic Doppler velocimeter (ADV), and turbidity at two elevations. Within the vegetation we measured velocity with

Table 1
Mean Water Depth and Height of SSC and Velocity Measurements at Unvegetated (U) and Vegetated (V) Stations[a]

Station	Mean depth m	SSC height mab	Velocity height mab
Lindsey Slough: 3–17 April 2017			
LiCh (U)	5.1	0.36	0.36
		0.91	0.10 to 0.80[b]
LiSo (V)	1.4	0.16	0.17
		0.40	0.44
		0.87	0.87
LiNo (V)	1.2	0.44	NA
LiE (V)	1.8	0.41	44
LiDs (U)	6.9	1.19	1.25 to surface[b]
Mokelumne River: 12–16 March 2018			
MkUs (U)	4.2	0.44	NA
MkT1 (U)	4.5	0.38	0.40
		NA	1.1 to 1.65[b]
MkT2 (V)	1.4	0.23	0.23
		0.88	0.89
MkT3 (V)	0.76	0.44	0.44
MkT5 (U)	4.5	0.40	0.40
		0.87	0.05 to 0.80[b]
MkTL (U)	4.5	0.2	NA
MkDs (U)	8.9	1.30	1.25 to surface[b]

[a]Heights in meters above the bed (mab). Water depth and temperature measured at all stations.
[b]Vertical profile.

ADVs at one to three elevations and turbidity at one or two elevations. In addition, an ADCP was deployed in the channel approximately one km down estuary of the Lindsey transect and one km up estuary of the Mokelumne transect to measure vertical profiles of current velocity. Data types and sampling volume elevations are provided in Table 1; for station coordinates and additional metadata see Lacy et al. (2020).

All instruments deployed within the patches were surrounded by cages to exclude vegetation from the sampling volumes. Nevertheless, vegetation caught on cages or frames both within and outside the patches interfered at times with acoustic or optical signals. These data were identified by low correlations or damped signals and were removed.

2.5. Time-Series Data Processing

We established coordinate systems with the x-direction (and u component of velocity) oriented along the channel and the flood direction positive. At the unvegetated channel stations LiCh and MkT5 (Figure 2), the shear velocity at the bed due to currents (u_*) was determined from the ADV data as the square root of the burst average of $u'w'$, where prime denotes turbulent fluctuations from the burst average. Hydrodynamic roughness z_0 was determined from u_* for each burst, assuming logarithmic velocity profiles, and we used the geometric mean of z_0 for $u_* > 0.005$ m / s as a representative hydrodynamic roughness $\hat{z}_0$ for each site. Bed shear stress due to currents was calculated as $\tau_b = \rho_w u_*^2$, where ρ_w is water density.

For unvegetated stations, depth-averaged velocity $\overline{u}$ was calculated from u_* and $\hat{z}_0$, assuming a logarithmic velocity profile. To determine the effect of the vegetation on currents, we predicted $\overline{u}$ in the absence of vegetation $\overline{u}_{p2}$ for the water depth (H) in the SAV, assuming a logarithmic profile, using the channel $\hat{z}_0$, and scaling $u_{*2} \sim u_{*1}\sqrt{H_2 / H_1}$, where subscript 2 denotes an SAV site and 1 denotes an adjacent channel site. The scaling assumes an equivalent along-channel pressure gradient at sites 1 and 2. $\overline{u}_v$, the depth-averaged along-channel velocity within the vegetation, was taken as the average of measured speeds below 0.9 mab in the SAV, excluding the uppermost measurements at MOK (MkT3) where the ADV was above the water surface at low tide. The attenuation in current speed attributable to vegetation is

$$A = 1 - \frac{\overline{u}_v}{\overline{u}_{p2}} \tag{1}$$

In determining the attenuation, data were restricted to periods with high data quality: April 6–12, 2017 for LS, March 13–16, 2018, and March 18–23, 2018 for MOK. At each site we used data from only one phase of the tide, avoiding an eddy that formed in LS during flood tides and flow diversion around the island at MOK during ebb tides.

The influence of vegetation on currents is commonly characterized by a bulk drag coefficient C_d, which is typically inversely related to the stem Reynolds number Re_d (Tanino & Nepf, 2008). We determined C_d from the MOK data, where the range of velocities was greater than at LS, from the momentum balance for the longitudinal exchange zone of submerged vegetation, between the horizontal pressure gradient and vegetative drag (Lightbody & Nepf, 2006; Nepf & Vivoni, 2000):

$$g\frac{d\eta}{dx} = -\frac{1}{2}C_d a \overline{u}_v^2 \tag{2}$$

where η is water surface elevation and g is the gravitational constant. In solving for C_d we estimated $d\eta / dx = u_{*1}^2 / H_1$, which assumes that the pressure gradient is balanced by bed friction in the unvegetated

channel. C_d was calculated for 0.1 m / s $< \overline{u} <$ 0.4 m / s and $H <$ 4.9 m at MkT5 during flood tides on the dates used for estimating attenuation. We calculated $Re_d = \overline{u}_v d_e / \nu$, where ν is the molecular viscosity of water.

Turbidity was measured with optical backscatter sensors (OBS) and converted to SSC using site-specific calibrations. To collect calibration samples, we mounted the OBS on a staff, deployed them from a small vessel in the channel at each study site, and pumped water samples from a port adjacent to the sensors. This procedure was repeated at various depths and tidal stages on the days before and after the deployments. Water samples were analyzed for SSC. Sensor-specific and site-specific calibration coefficients were determined by least-squares-fit linear regression between the OBS voltage and the SSC. The coefficient of determination R^2 was greater than 0.98 for each of the eight OBS deployed in LS and greater than 0.9 for each of the nine OBS deployed at MOK. For MOK, the calibrations were based on samples with SSC $<$ 35 mg / L because the calibrations shifted at higher SSC, likely due to an increase in suspended-particle size. We did not have enough data to develop separate calibrations for high concentrations. As a result, SSC values above 35 mg / L are underestimated.

We determined vertical profiles of SSC in the channel based on the Rouse equation:

$$\mathrm{SSC}(z) = \mathrm{SSC}_r \left(\frac{z}{z_r} \right)^{-\beta} \tag{3}$$

where SSC_r is the SSC at a reference elevation z_r, z is the elevation above the bed, $\beta = w_s / \kappa u_*$, $\kappa = 0.41$ is the von Karman constant, and settling velocity w_s was determined for the median particle size in suspension, as described below.

2.6. Particle Size in Suspension and Settling Velocity

The particle size in suspension differed from that on the bed because smaller particles are more easily resuspended and because much of the suspended sediment in the Delta is mud, which tends to aggregate into larger flocs. We measured the size distribution of particles in suspension during each deployment by submerging a Laser In-Situ Scattering and Transmissometry instrument (LISST) to several depths in the channel (profile data). In addition, during the MOK deployment we collected time-series data with a LISST at 0.5 m above the bed at station MkTL (Figure 2).

The vertical distribution of sediment (Equation 3) depends on the settling velocity w_s. For the Mokelumne River, we computed w_s from the time series of particle size distributions at MkTL. First, we computed the relative floc density $\Delta\rho_f$ at each point in time, from the ratio of mass concentration (SSC) measured by the OBS to volume concentration of particles measured by the LISST (Mikkelsen & Pejrup, 2001). Then, we determined the fractal dimension n_f for the deployment from the log-log fit between $\Delta\rho_f$ and the median particle diameter D_{50} in suspension. In fitting, fractal dimension was limited to values between 2 and 3; n_f values between 1 and 2 are typical of fragile open-ocean aggregates (Baugh & Manning, 2007), and these estuarine flocs were unlikely to be extremely fragile. The resulting best-fit n_f was 2.2, at the low end of values previously reported for San Francisco Bay (Allen et al., 2019; Manning & Schoellhamer, 2013).

Settling velocity and particle Reynolds number Re_p were computed iteratively:

$$w_s = \frac{(\rho_s - \rho_w) g}{18\mu} D_p^{3-n_f} \frac{D_{50}^{n_f - 1}}{1 + 0.15 Re_p^{0.687}}, \quad Re_p = \frac{w_s D_{50}}{\nu} \tag{4}$$

(Winterwerp, 1998), where sediment density $\rho_s = 2.65 \times 10^3$ kg / m^3, water density $\rho_w = 1.1 \times 10^3$ kg / m^3, molecular viscosity $\mu = 1.14 \times 10^{-3}$ kg / ms, kinematic viscosity $\nu = 1.14 \times 10^{-6}$ m^2 / s, and we set the primary particle size $D_p = 10$ μm (the median disaggregated particle size of the bed sediments within the vegetation at MOK) as representative of sediment transported in suspension. For sand at MOK, we iteratively solved for Re_p and w_s for specific particle diameters (Fredsoe & Deigaard, 1992). For Lindsey Slough, we used the LISST profile data to determine w_s with Equation 4. We set n_f to 2.2, based on the Mokelumne data,

rather than deriving n_f from the limited LS data, and set $D_p = 4$ μm, reflecting the finer bed sediments in the LS vegetation.

3. Results

3.1. Conditions During the Deployments

The winter preceding the April 2017 deployment in Lindsey Slough was the second wettest on record in northern California, with very high flows in the Sacramento River (Singh et al., 2018). These conditions typically result in the deposition of fine sediment in backwater environments like LS. However, during the deployment, currents in Lindsey Slough were dominated by tides, with no noticeable influence of elevated river discharge. The tide range was approximately 1 m. Current velocity in the channel varied from –0.20 to 0.25 m / s, with flood tides slightly stronger and shorter than ebb tides (Figure 3). Hydrodynamic roughness $\hat{z}_0$ was 8×10^{-5} m. Maximum current speed within the vegetation was less than 1 cm / s. SSC at LiCh varied tidally between 5 and 25 mg / L, with maximum SSC at high tide due to advection of an along-channel gradient in SSC, with greater SSC bayward where tidal currents are stronger and wind waves resuspend sediments in flooded shallows (Figure 3c).

At the Mokelumne River in March 2018, tide range was approximately 1 m and depth-averaged currents at MkDs ranged from –0.5 to 0.5 m / s at the beginning of the deployment, with longer and slightly stronger ebb than flood tides (Figure 4). Two precipitation events influenced Mokelumne River discharge during the deployment. During the first (March 17–19) event, ebb-tide current speed and SSC increased slightly. The second (March 23–26) event was more substantial, raising water levels and producing continuous downstream flows for two tidal cycles, with ebb-tide speeds up to 0.8 m / s. In Mok $\hat{z}_0$ was 3.8×10^{-3} m, two orders of magnitude greater than in LS, due to coarser bed sediments and regular bedforms. SSC in the channel ranged from 5 to 20 mg / L during low flows, with the highest concentrations during ebb tides, and increased with current speed and river discharge (Figure 4d). Vegetation caught on frames affected data quality; at some sites poor data quality was intermittent, but at MkT5 data quality was low for March 24–26.

3.2. Vegetation Density, Frontal Area, and Areal Density

The submerged vegetation appeared to be very dense at all sites (Figure 5a). Mean dry biomass density ranged from 218 g / m^2 in Middle River to 596 g / m^2 in Lindsey Slough. Biomass density was not significantly different between Lindsey Slough and the two Mokelumne River patches and was lower in Middle River (Figure 5b). The slope m_v of plant area versus biomass was 0.017 m^2 / g (95% confidence interval 0.014–0.019 m^2 / g), with the intercept not significantly different from zero (Figure 5c). Frontal area a was 5.8 m^{-1} for LS and 6.5 m^{-1} for MOK-north, averaged over vegetation height. The greater a (despite lower biomass density) at MOK than LS is due to the lower h_v at MOK than at LS. Mean effective diameter d_e was 9.7 mm (s.d. 1.8 mm, $N = 10$), more than three times greater than the average stem diameter of 2.7 mm. Areal density ϕ was 0.044 for LS and 0.050 for the MOK.

For most of the tidal cycle, the *E. densa* canopies at the study sites reached the water surface. Although from an ecological perspective *E. densa* is submerged, from a hydrodynamic perspective it functions like emergent vegetation as long as it occupies the entire water depth ($H / h_v = 1$, where H is water depth). In emergent vegetation, the horizontal pressure gradient is balanced by vegetative drag, and velocity is constant over depth for vertically uniform plant density (Lopez & Garcia, 2001; Nepf & Vivoni, 2000). At high tide, $H / h_v > 1$ at our study sites, and the *E. densa* became hydrodynamically submerged.

3.3. Bed Sediment Grain Size and Bulk Density

Bed sediment grain size in the channel (outside the SAV) was quite different at the three sites: At Lindsey Slough the sediments were 100% fines (< 63 μm diameter), at Middle River they were 76% fines and 24% sand, and at Mokelumne River sediments were 3.7% fines and 96.3% sand (Figure 6). The coarser sediments at MOK reflect the stronger currents at the site, especially during periods of elevated river discharge, and

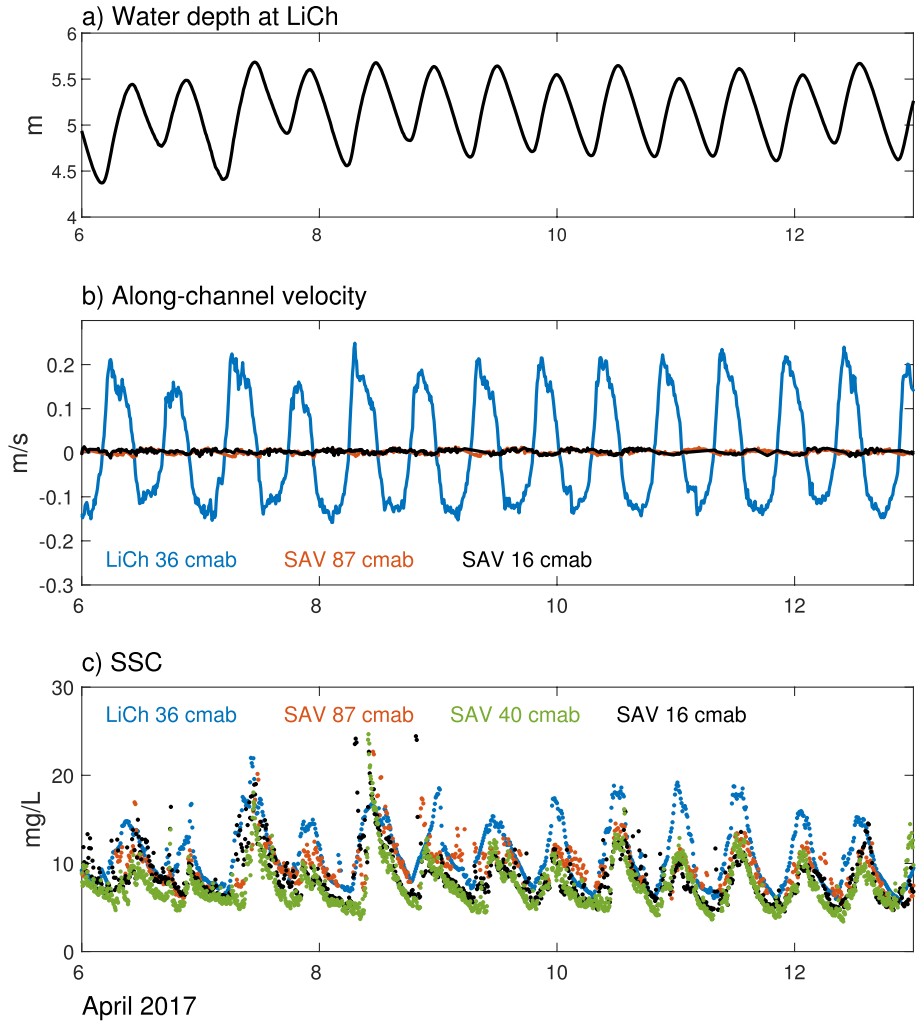

Figure 3. Water level, current velocity, and suspended-sediemnt concentration (SSC) in Lindsey Slough, April 7–13, 2017. (a) Water depth at station LiCh (Figure 2a), (b) along-channel velocity in the unvegetated channel (LiCh) and two elevations within the adjacent vegetation, (c) SSC at LiCh and three elevations within the adjacent vegetation.

the proximity to the head of the tide. The fine sediments at LS are consistent with the lower tidal current speeds and the small, low-gradient watershed of this backwater. Middle River is influenced by high flows in the San Joaquin River but is farther down estuary than MOK, so much of the sand supplied by the watershed settles out upstream of MR.

In contrast, within the vegetation, the median grain size D_{50} was less than 10 μm at all three sites (Figure 6). The range of grain sizes in the channel at MOK and MR was narrow and overlapped little with the fine particle sizes within the vegetation. This separation indicates that fine particles largely remain suspended by tidal currents in the channels, only settling out in the SAV where currents are attenuated. In Lindsey Slough, where currents are not strong enough to resuspend sediments, grain size distribution was almost identical within and outside the vegetation. Little sand is transported to LS, and the flocs in suspension settle out both in the channel and in the vegetation. Mean dry bulk density in the channels was directly related to D_{50}, whereas within the SAV it was low at all sites, reflecting both finer particle sizes and less compaction than outside the vegetation (Figure 6e).

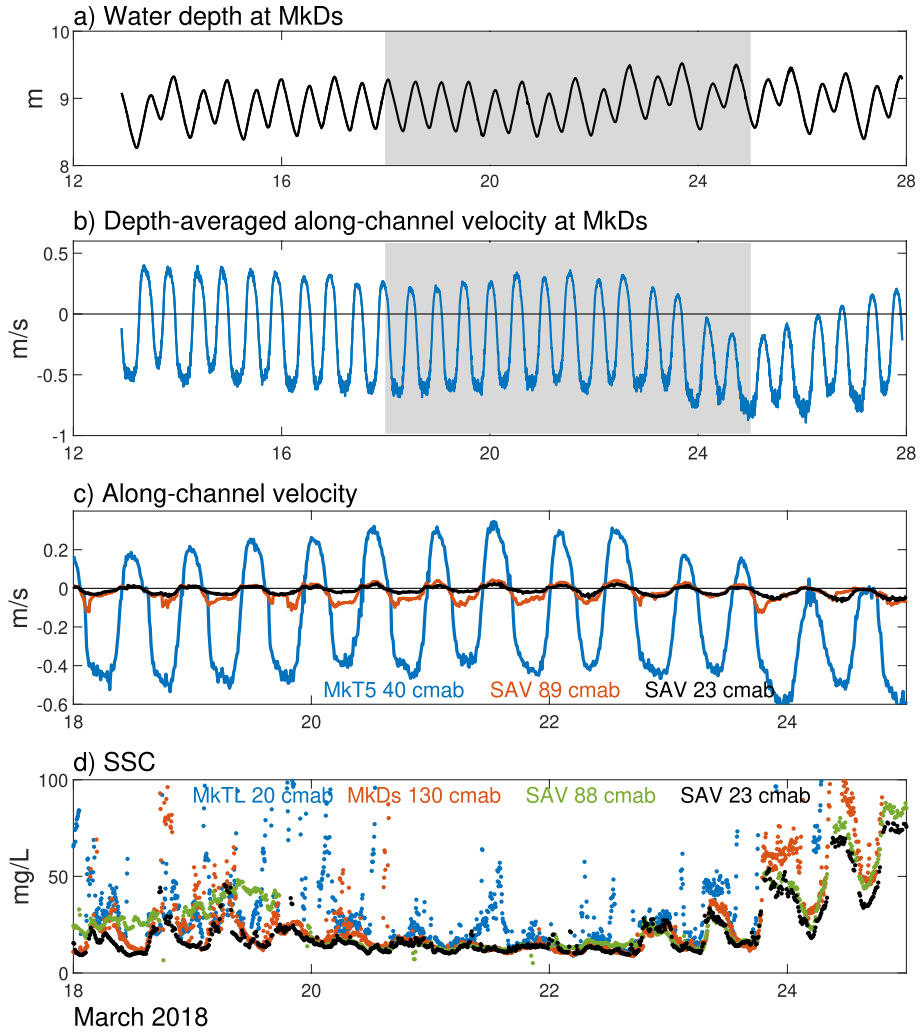

Figure 4. Water level, current velocity, and suspended-sediment concentration (SSC) in the lower Mokelumne River, March 2018. (a) Water depth at station MkDs, March 12–28, (b) depth-averaged along-channel velocity in the unvegetated channel (MkDs), (c) along-channel velocity in the unvegetated channel (MkT5) and at two elevations within the adjacent vegetation, (d) SSC in the channel at MkTL (0.2 mab) and MkDs (1.3 mab) and at two elevations within the adjacent vegetation. Shading in panels (a), (b) shows time period covered by panels (c), (d). For station locations see Figures 2d and 2e.

3.4. Current Attenuation by *E. densa*

Current speed within the vegetation was an order of magnitude lower than depth-averaged along-channel velocity $\overline{u}$ at the channel stations (LiCh, MkT5) (Figures 7a and 7b). At LS, current speed in the SAV did not vary vertically. LiE is included in Figure 7a, even though LiCh is not a particularly good reference site for LiE, to illustrate that current speed in the SAV was as slow at LiE as at LiSo. At MOK, currents were stronger higher up in the canopy, suggesting that plant density decreased near the water surface, consistent with the highly variable plant size in the MOK patch.

Vegetative attenuation A of along-channel velocity was calculated for flood tides at MOK with channel $\overline{u}$ greater than 6 cm / s. We did not calculate A for LS because of differences in tidal phase between the channel and the SAV. A was greater than 90% for all channel $\overline{u}$, while decreasing slightly at higher velocities (Figure 8a). Vegetative drag coefficient C_d was inversely related to stem Reynolds number Re_d, as expected (Figure 8b). A log-log regression fitting $C_d = \alpha Re_d^{\beta}$ yielded $\alpha = 10^{2.24\pm0.11}$ and $\beta = -1.46 \pm 0.054$ ($R^2 = 0.70$), corresponding to C_d of 2.2 (range 1.5–3.3) at $Re_d = 20$ and 0.04 (range 0.025–0.072) at $Re_d = 300$. Thus, C_d

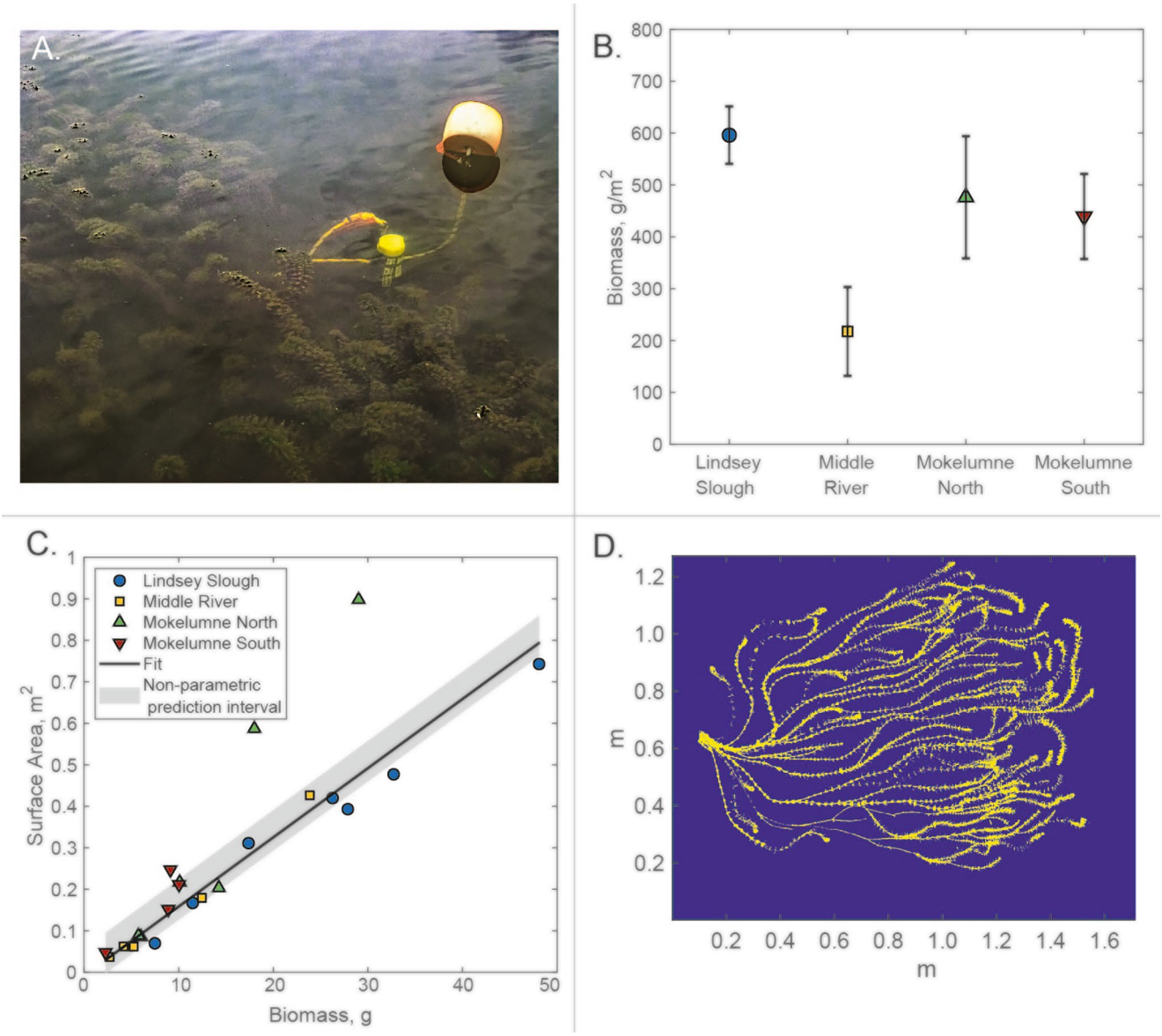

Figure 5. Vegetation density. (a) Photograph of submerged *E. densa* and pressure sensor in the Middle River, (b) mean ± standard error of dry biomass per m^2 at the study sites, (c) area versus biomass for the individual plants harvested at each site, with slope determined by repeated medians method, (d) binary image of *E. densa* plant collected in Lindsey Slough.

was usually lower than the asymptotic value for rigid cylinders of 1.0 (Tanino & Nepf, 2008). Unlike the case of rigid cylinders, C_d did not asymptote at high Re_d perhaps because at higher current speeds, pronation of flexible vegetation decreases drag, which is not accounted for in Equation 2 (Luhar & Nepf, 2013; Vargas-Luna et al., 2015). Our observations fell within the wide range of C_d that has been reported for flexible vegetation (Sukhodolova & Sukhodolov, 2012; Vargas-Luna et al., 2015).

At high tide or during high river flows at MOK, water depth exceeded the plant height and some flow passed over the canopy. These conditions are discussed in Section 3.7.

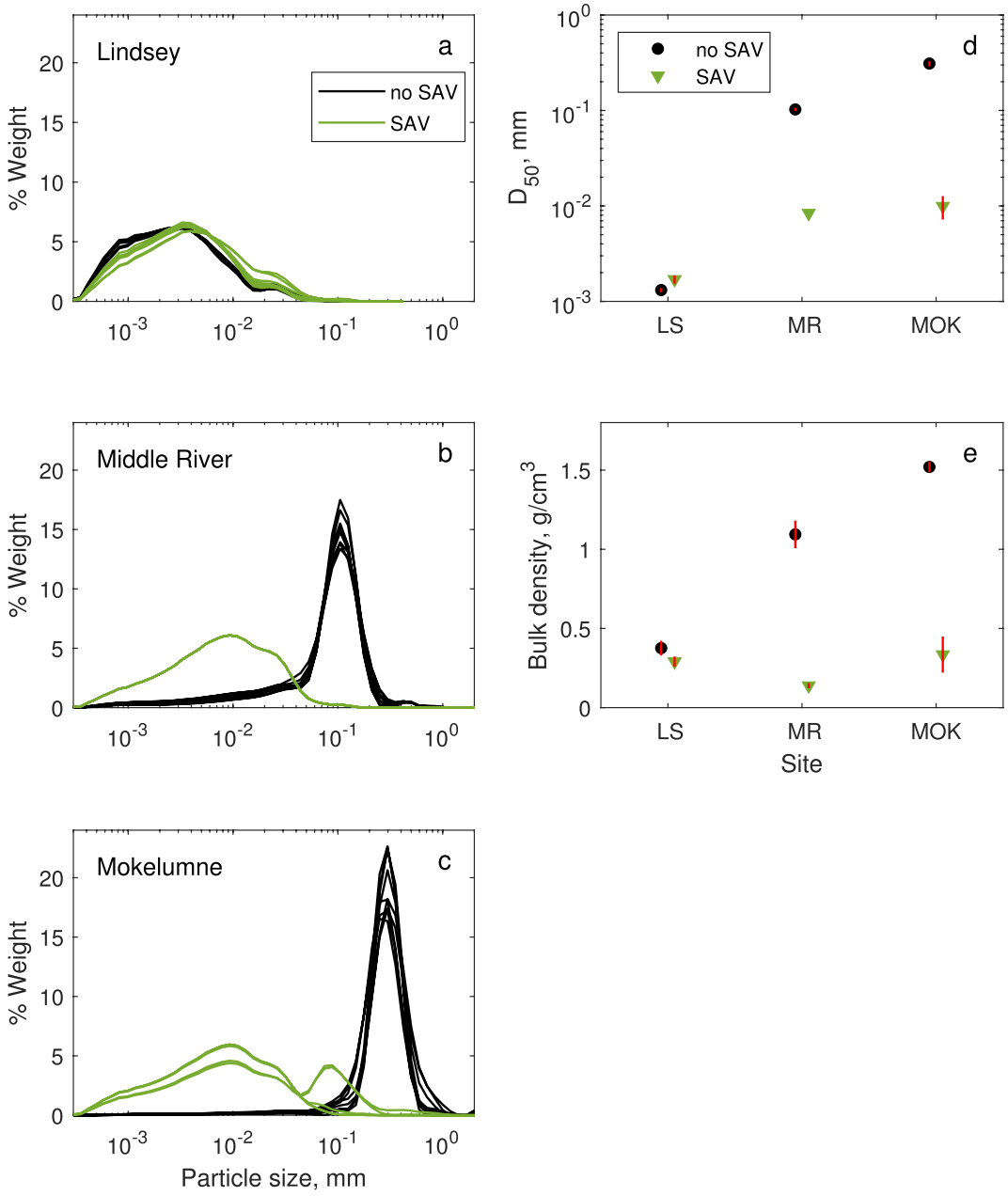

Figure 6. Properties of surficial 1 cm of bed sediments within and outside vegetation patches at the three sites. Disaggregated particle size distribution in (a) Lindsey Slough, (b) Middle River, and (c) Mokelumne River, (d) median particle size D_{50} (mean ± standard deviation (s.d.)) (at MR particle size distribution was analyzed for a composite of five samples from within the submerged aquatic vegetation, so s.d. could not be calculated), and (e) dry bulk density (mean ± s.d.).

3.5. Particle Size in Suspension and Settling Velocity

In Lindsey Slough, the median D_{50} of particles in suspension was 24 μm, indicating a moderate level of flocculation compared to the D_p of 4 μm. The settling velocity w_s associated with the median particle size was 1.1×10^{-4} m / s. In a typical water depth of 1.4 m within the *E. densa* patches, these particles would settle from the water surface to the bed in 212 min. We speculate that flocculation in the quiescent patches may increase particle size and decrease settling time.

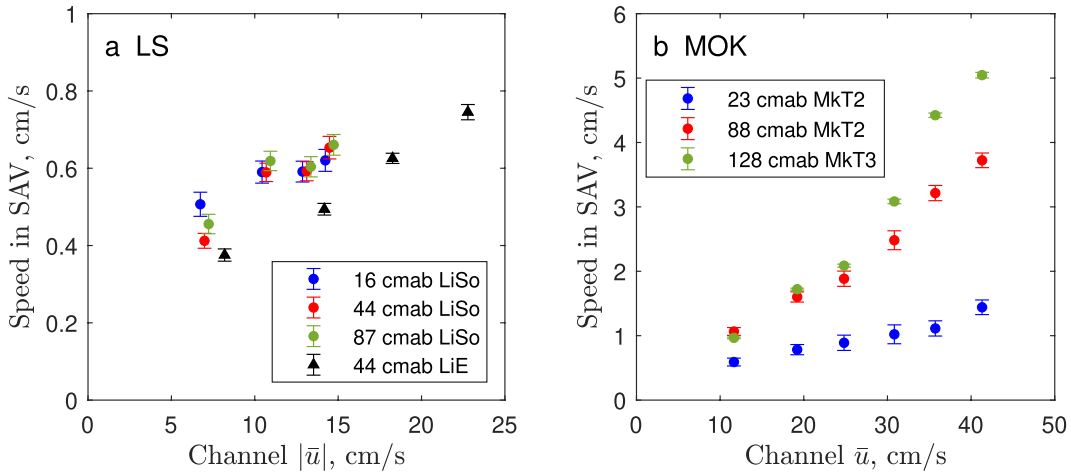

Figure 7. Current speed within the vegetation (bin average ± standard error) at four elevations above the bed (cmab) versus depth-averaged along-channel velocity $\bar{u}$ at the channel stations in (a) Lindsey Slough (ebb tides) and (b) Mokelumne River (flood tides). Data binned by $\bar{u}$.

The median D_{50} of particles in suspension in Mokelumne was 74 μm, with w_s of 8.6×10^{-4} m / s during the low flow conditions of March 15–22, 2018. The settling time for a quiescent 1.4 m water column is 27 min. During the high flows of March 23–26, the D_{50} of particles in suspension increased, and during ebb tides particle size distributions were bimodal, suggesting that some of the suspended sediment was sand. Indeed, suspended sediment in a water sample collected 1 m below the surface during ebb tide on March 27 was 12% sand (SSC 53 mg / L). For this higher discharge period, we assumed w_s of 8.6×10^{-4} m / s for flocs and also considered vertical mixing of two classes of sand: 320 μm particles (D_{50} of the Mokelumne channel bed sediments) with w_s of 4.1×10^{-2} m / s and 100 μm particles with w_s of 5.9×10^{-3} m / s.

3.6. Influence of *E. densa* on Suspended-Sediment Concentration

The influence of *E. densa* on SSC varied with tidal phase and SSC in the unvegetated channel SSC_u (measured at LiCh in LS and MkTL in MOK). At both sites, there was little difference between SSC_u and SSC within patches (SSC_v) at low concentrations. For the highest SSC_u class in Lindsey Slough (15–18 mg / L), mean

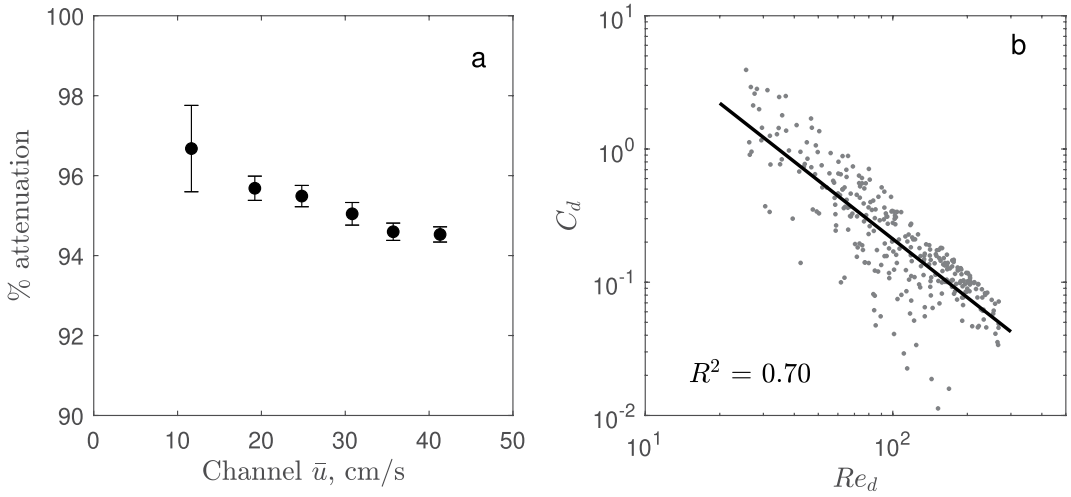

Figure 8. (a) Attenuation of along-channel velocity (bin average ± standard error) by vegetation. (b) Vegetative drag coefficient C_d versus stem Reynolds number Re_d, with least-squares-fit regression line. Data from the Mokelumne River, flood tides ($N = 313$).

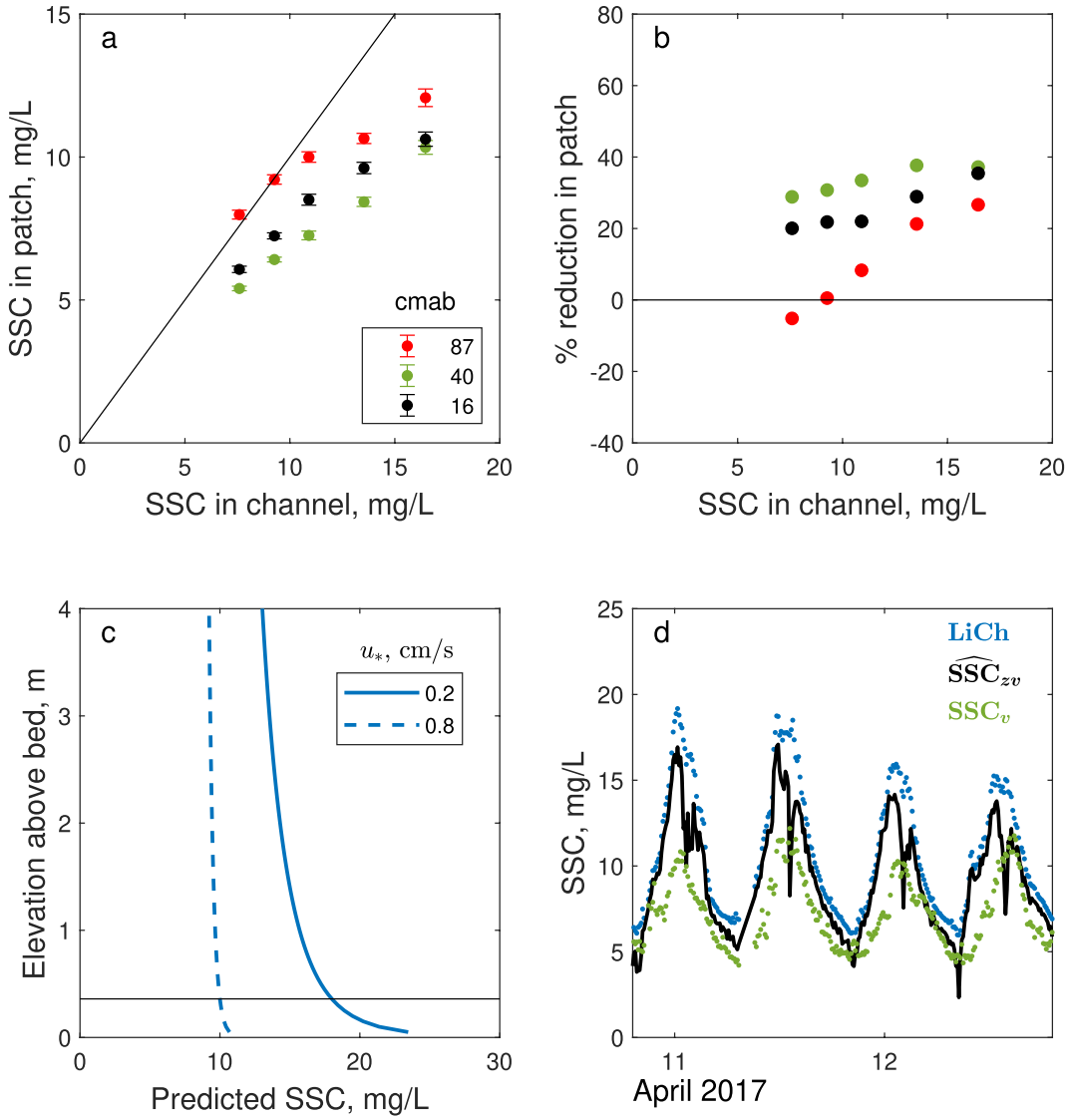

Figure 9. Effect of *E. densa* on suspended-sediment concentration (SSC) in Lindsey Slough. (a) SSC (bin average ± standard error) within the submerged aquatic vegetation (SAV) at three elevations above the bed (cmab) versus SSC at 36 cmab at LiCh. Data binned by SSC at LiCh. (b) Percent reduction in SSC within SAV. (c) Predicted vertical profile of SSC for flocs with $w_s = 1.1 \times 10^{-4}$ m / s for SSC at LiCh of 18 mg / L and u_* of 0.2 cm / s (solid) and SSC at LiCh of 10 mg / L and u_* of 0.8 cm / s (dashed). Horizontal line indicates measurement elevation. (d) SSC 36 cmab (LiCh), predicted SSC 3.8 mab ($\widehat{SSC}_{zv}$), and average of SSC at 16 and 40 cmab in the SAV, April 11–12, 2017.

SSC_v was 26%–38% lower than SSC_u, depending on elevation within the vegetation (Figures 9a and 9b). At Mokelumne, the range of SSC_u was greater, and for the highest class (45–55 mg / L), mean SSC_v was 47%–57% lower than SSC_u (Figures 10a and 10b). At both sites there was less reduction in SSC higher up in the canopy.

E. densa inhabits shallow water, so advection into patches originates from the near-surface waters of the channel, where SSC may be lower than at the near-bed measurement elevations. To distinguish the effect of vegetation from that of elevation, we predicted SSC in the channel at the SAV elevation (3.8 mab at LiCh, 3.5 mab at MkTL) from Equation 3 ($\widehat{SSC}_{zv}$). The fraction C of near-bed channel SSC that remains in suspension in the vegetation is the product of a normalized SSC in the channel at the elevation of the vegetation C_{zv} (elevation effect) and a normalized SSC within the vegetation C_v (vegetation effect):

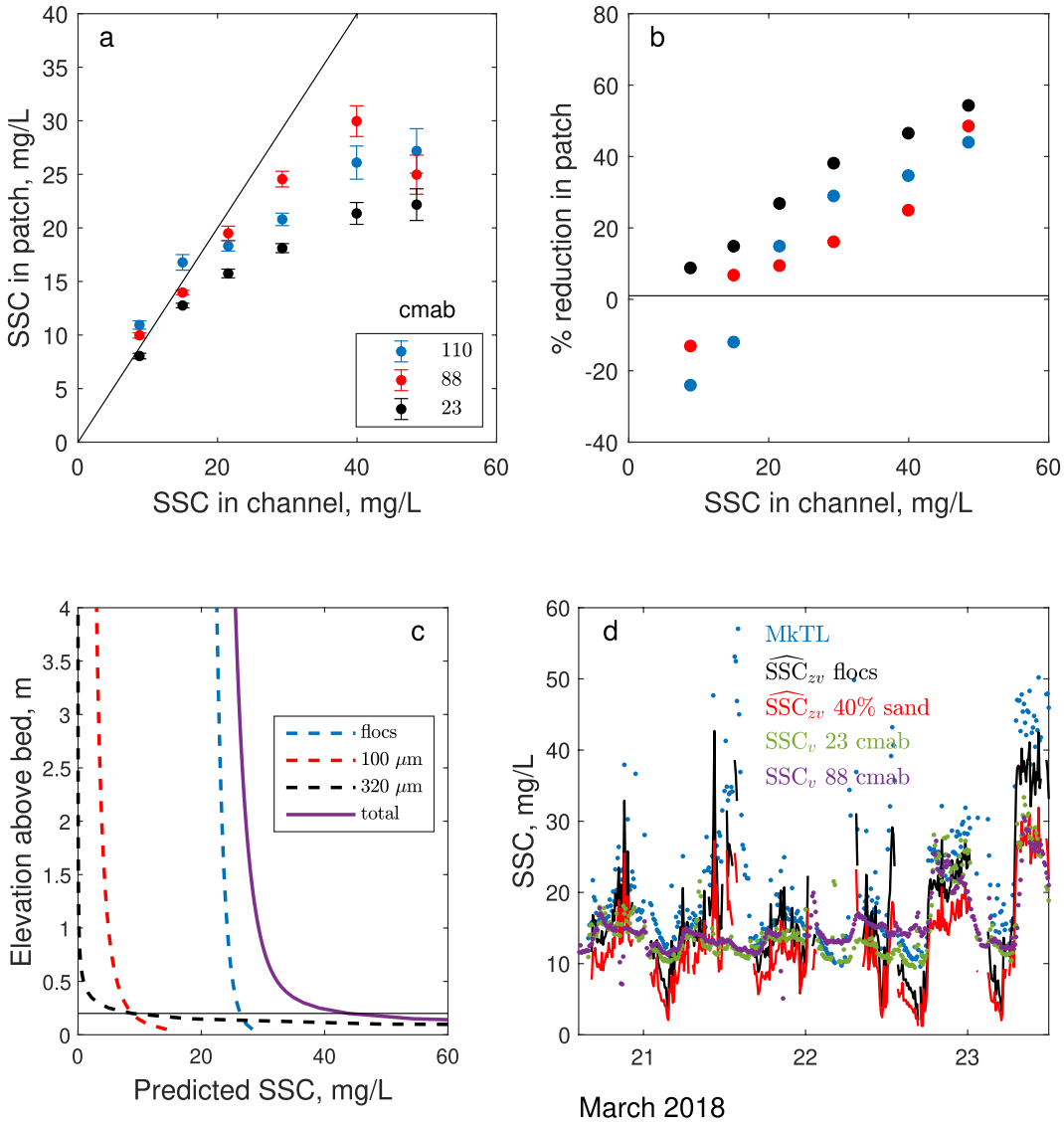

Figure 10. Effect of *E. densa* on suspended-sediment concentration (SSC) in the Mokelumne River. (a) SSC (bin average ± standard error) within the SAV at three elevations above the bed (cmab) versus SSC at 20 cmab in the unvegetated channel (MkTL). Data binned by SSC at MkTL. (b) Percent reduction in SSC within *E. densa*. (c) Predicted vertical distribution of flocs ($w_s = 8.6 \times 10^{-4}$ m / s), 100 μm sand ($w_s = 5.9 \times 10^{-3}$ m / s), and 320 μm sand ($w_s = 4.1 \times 10^{-2}$ m / s) (dashed) and total SSC (solid) for mixture of 40% sand and 60% flocs with SSC of 44 mg / L at 20 cmab. Horizontal line indicates measurement elevation. (d) SSC at MkTL, $\widehat{SSC}_{zv}$ for flocs and mixture of 40% sand and 60% flocs, and SSC_v at three elevations above the bed, March 21–23, 2018.

$$C = SSC_v \,/\, SSC_u = \widehat{SSC}_{zv} \,/\, SSC_u \times SSC_v \,/\, \widehat{SSC}_{zv} = C_{zv} \times C_v \tag{5}$$

Vegetative trapping is $T_v = 1 - C_v$.

In Lindsey Slough, C_v averaged across 6 days was 0.82, indicating that 18% of the sediment transported into the patch was retained by trapping or settling (Figure 9d). C_v was lower during flood than ebb tides. During ebb tides, the temporal decay in SSC_v and $\widehat{SSC}_{zv}$ was similar, reflecting settling both within and outside the vegetation. During flood tides, the advectively driven increase in SSC in the channel was muted and delayed in the vegetation. The importance of vertical mixing in the channel also varied tidally. For a typical flood or ebb tide shear velocity u_* at LiCh of 0.8 cm / s, SSC_u of 10 mg / L, and $w_s = 1.1 \times 10^{-4}$ m / s, Equation 3

predicts that the flocs are well mixed vertically, with $C_{zv} = 0.92$ (Figure 9c, dashed). C_{zv} decreased to 0.73 during high slack tides, when SSC_u was greatest (18 mg / L) and vertical mixing was weak ($u_* = 0.2$ cm / s) (Figure 9c, solid). C_v was also lowest (T_v greatest) during high slack tides (Figure 9d).

At Mokelumne River, C_v was more difficult to determine because the particle size in suspension varied during the deployment. For the median floc size ($w_s = 8.6 \times 10^{-4}$ m / s) and u_* of 2.3 m / s (typical during low flows), C_{zv} was 0.77, accounting for essentially all of C at the lowest concentrations. Average C_v for 20 mg / L < SSC_v < 30 mg / L was 0.86. At higher elevations in the patch, SSC_v was at times greater than SSC_u, perhaps due to remobilization of sediment previously trapped on vegetation. When river discharge was elevated (March 23–26), SSC_u increased during strong ebb tides and both flocs and sand were in suspension. For these higher concentrations (e.g., 44 mg / L), C was 0.5 (Figure 10b). The proportion of this 50% reduction attributable to T_v is inversely related to the assumed percent sand in SSC_u. For u_* of 4.0 cm / s (typical of high-flow ebb tides), with no sand in suspension C_{zv} is 0.86 and C_v is 0.56 ($T_v = 0.42$), whereas for 40% sand (assumed in this example to be half 320 μm and half 100 μm particles), C_{zv} is 0.41 (Figure 10c) and C_v is 0.85 ($T_v = 0.15$). We expect that sand in suspension never exceeded 40% during the deployment and was usually lower. C was lowest during high-discharge ebbs, when some sand was likely in suspension (Figure 10d, March 23). Fine sand (100 μm) transported into the vegetation would settle out quickly: In a 1.4 m deep patch it would travel only 4.7 m (at 0.02 m / s) before depositing on the bed.

In summary, at the Mokelumne River site, T_v was 0–0.15 for SSC_u < 30 mg / L, which characterized 69% of the deployment, and 0.15–0.40 when the discharge and SSC_u were elevated. The variation in vegetative trapping of suspended sediment with tidal phase and river discharge makes it difficult to estimate a long-term mean T_v from this data set and reflects the dependence of trapping processes on flow and turbulence within patches as well as particle size and density.

3.7. Currents and Sediment Transport at High Water

Water depth exceeds the vegetation height for three to four hours daily at high tidal stages at both LS and MOK and for longer periods during high river flows at MOK. Because flow is strongly attenuated within *E. densa*, flow over the canopy provides an important pathway for sediment to be advected over and settle farther into the vegetation. Marshes are only inundated at high water levels, so sediment transport under these conditions is especially relevant to marsh sediment supply.

Submerged vegetation is classified as dense, meaning that a mixing layer with an inflection point in the mean velocity forms at the top of the canopy, for $C_d a h_v > 0.1$ (Nepf, 2012). $C_d a h_v$ exceeded this threshold for all conditions at both the sites. However, full development of mixing layers over submerged vegetation requires $H / h_v > 2$ (Nepf & Vivoni, 2000), which never occurred at our study sites. The vegetation inhabited regions with mean water depth ranging from 0.5 to 2 m. At the primary instrumented SAV stations at both sites, mean water depth was 1.4 m and maximum H / h_v was approximately 1.15 during typical high tides. To investigate the potential for flow and sediment transport over the canopy during high tides, we assess three cases: typical high tides at LS and at MOK, and the 23–25 March high flows at MOK (Mok-hi), when H / h_v reached 1.27.

The ratio of the height of penetration to the canopy height h_p / h_v increases with frontal area a and decreases with submergence depth (Nepf & Vivoni, 2000). For typical high tides at LS and MOK, h_p / h_v was approximately 0.84, and for Mok-hi h_p / h was approximately 0.75, based on results in Nepf & Vivoni (2000) for $a = 5.5\ \mathrm{m}^{-1}$. We estimated flow speed above the canopy assuming a modified logarithmic velocity profile, displaced from the bed by an elevation d (Lacy & Wyllie-Echeverria, 2011; Luhar & Nepf, 2013):

$$u(z) = \frac{u_{*v}}{\kappa} \ln \frac{z - d}{z_{0v}} \tag{6}$$

where $d = (h_v + h_p) / 2$ (Nepf & Vivoni, 2000), hydrodynamic roughness at the canopy top z_{0v} was set at 0.03 m (Lacy & Wyllie-Echeverria, 2011; Nepf & Vivoni, 2000), and u_{*v} is the shear velocity at the canopy top. We estimated $u_{*v} = u_{*1}\sqrt{(H_2 - h_v) / H_1}$, where 1 and 2 indicate channel and SAV sites, which assumes

Table 2
Input Parameters and Results for Modified Log Layer Above the Canopies at High Tide

Site	H_1 m	u_{*1} m/s	H_2 m	d m	u_{*v} m/s	u_h m/s	u_{max} m/s
LS	5.6	0.009	1.9	1.52	0.0024	0.008	0.015
MOK	5.0	0.03	1.9	1.52	0.0083	0.028	0.052
MOK-hi	5.2	0.05	2.1	1.44	0.018	0.084	0.13

Note. Results Water depth H_1 and shear velocity u_{*1} at channel sites, water depth H_2 at vegetated sites, displacement elevation d, shear velocity above canopy u_{*v}, predicted velocity at the top of the canopy u_h, and predicted velocity at the water surface u_{max}, from Equation 6. Hydrodynamic roughness above the canopy z_{0v} is 0.03 m for all cases.

that the along-channel pressure gradients at the channel site and over the vegetation were the same. For each case, u_{*1} was set to the maximum u_* measured in the channel during water depths within 0.2 m of high tide.

In Lindsey Slough, current speed above the canopy is limited to 0.008–0.015 m / s by the drag exerted by the vegetation (Table 2). While low, these speeds are 2–3 times greater than within the canopy (Figure 7a). If directed toward shore, particles advected at 0.012 m/s would cross the 18 m width of the SAV and reach the marsh in 1,500 s, which is much shorter than the duration of $H > h_v$. Particles with $w_s = 1.1 \times 10^{-4}$ m / s settle only 0.17 m in 1,500 s, suggesting that at high tide, when the water surface is 0.25 m above the SAV, water would reach the marsh edge with less depletion in SSC than occurs within the vegetation.

At MOK, predicted current speeds over the vegetation are greater than in LS (Table 2). For Mok-hi, with a velocity of 0.1 m / s and $w_s = 8.6 \times 10^{-4}$ m / s, flocs could be transported up to 47 m before settling through the 0.4 m of water above the canopy, farther than the width of most marsh-fringing patches. In addition, turbulence generated at the canopy–water interface could mobilize sediment trapped in the upper canopy. These processes may contribute to the greater observed SSC at higher elevations in the SAV (Figure 10a).

4. Discussion

4.1. Influence of Hydrodynamic Setting and Season on Sediment Trapping

Sediment is trapped by SAV because lower current speeds within the vegetation increase settling and decrease erosion (Madsen et al., 2001). The higher-energy Mokelumne River site illustrates both of these processes. In the channel, bed shear stress keeps flocs in suspension for much of the tidal cycle, whereas in the slower currents within the SAV they settle out. The differential trapping produces particle size sorting, with much finer bed sediments within patches than in the MOK channel (Figure 6). The retention of fines and associated organic matter within patches benefits the SAV, promoting colonization.

In contrast, at LS, with $\tau_b < \tau_c$ throughout the tidal cycle, there is no erosion for the SAV to decrease, but SAV increases settling by reducing transport distance. Within patches, where current speed is reduced by 90% and water depth is three times lower than in the channel, particles are transported approximately 3% as far as in the channel before depositing, and may be trapped directly on vegetation over shorter distances. For the muddy LS channel sediments, there was almost no difference between particle size within and outside patches, consistent with observations in muddy sites with dense SAV by van Katwijk et al. (2010). In lower-energy muddy sites, water depth and its influence on light penetration are likely more important controls on colonization than bed sediment properties.

Previous studies have shown that biomass density of some species of SAV is inversely related to current strength for speeds above 0.1 m / s, which would result in less trapping, or even erosion, at more energetic sites (Chambers et al., 1991; Madsen et al., 2001). In this study plant density did not differ significantly between the sites, consistent with the lack of influence of current speed on the probability of occurrence of *E. densa* in the Delta (Durand et al., 2016). During low flows, when suspended sediment is dominated by flocs, the rate of vegetative sediment trapping T_v averaged 0.18 at LS and was somewhat lower at MOK. T_v increased during higher discharge at MOK, exceeding that at LS at the times of greatest SSC. The combination of greater T_v with greater SSC_u during elevated discharge, which occurs intermittently at MOK, suggests the potential for a greater rate of sediment accretion at higher energy sites. Measurements of long-term accretion support this conclusion: The rate of inorganic sedimentation was greater in cores collected within *E. densa* patches in MOK than in LS (Drexler et al., 2021).

Our study took place during the active growing season of *E. densa*. Sediment trapping by SAV is likely to vary seasonally, not only in magnitude but also potentially in sign. In the upper Chesapeake Bay, turbidity

was greater inside than outside SAV, indicating erosion in the SAV, after major storm events that removed leaves and plants (Gurbisz et al., 2016). In seagrass meadows, seasonal decrease in plant density has been associated with increased SSC and erosion (Bos et al., 2007; Hansen & Reidenbach, 2013). These studies show that sediment storage in and release from SAV can be cyclical, serving as much to alter the timing of turbidity peaks and sediment transport as to increase long-term sediment retention. Most of the sediment supplied to the Delta (e.g., 82% for 1998–2002) is associated with high-flow events during the wet winter or spring runoff (Wright & Schoellhamer, 2005). Thus storage and release of sediment by Delta SAV may vary seasonally and on event timescales, particularly at sites with strong riverine influence such as MOK.

4.2. Influence of *E. densa* on Channel SSC and Suspended-Sediment Flux

In channels fringed by invasive SAV, vegetative sediment trapping is limited by slow current speeds within the canopies and the low settling velocity of flocs. By strongly attenuating currents, *E. densa* effectively reduces the cross-sectional area of channels and deflects flow and suspended-sediment flux (SSF) into the unobstructed central channel. In the middle of the channel, water and sediment flux are directed almost entirely along channel, but at the edge of the vegetation the lower velocity within the SAV produces a lateral component of flux. Although this lateral velocity is small (estimated $< 10^{-3}$ m / s), it is an important driver of SSF into SAV because it acts along the length of the fringing vegetation.

We examine these effects in more detail for the study transect in Lindsey Slough (Figure 2b), where the channel cross-section is well constrained and the distribution of vegetation along the channel margins is typical. SAV occupied 16% of the cross-sectional area of the channel, or, equivalently, the blockage factor B_x was 0.16 (Luhar & Nepf, 2013). Assuming no change in tidally driven water flux and no morphologic adaptation, which is reasonable for the LS channel where τ_b is low, the reduction in channel area has increased cross-sectionally averaged velocity by 19.5%.

To assess the channel-scale impact of SAV, we compare sediment trapping in SAV to SSF in the channel over a tidal cycle. SSF per m of channel width at LiCh is

$$\mathrm{SSF_m} = \overline{u}\overline{H}\overline{c}$$

where c is SSC and $\overline{c}$ was calculated from profiles predicted by Equation 3. We estimated SSF for the unvegetated cross-section, denoted $\mathrm{SSF_A}$, by multiplying $\mathrm{SSF_m}$ by the ratio of the area of the unobstructed channel to that of the 1-m wide water column at LiCH at mean water depth. For April 6–13, average cumulative flood tide $\mathrm{SSF_A}$ was 6,390 kg, and the tidal average $\langle \mathrm{SSF_A} \rangle$ was 1,970 kg in the flood direction per semidiurnal tidal cycle (31% of the flood-tide $\mathrm{SSF_A}$. The landward $\langle \mathrm{SSF} \rangle$ is produced by an along-channel gradient in SSC, increasing toward the estuary, and is consistent with the landward $\langle \mathrm{SSF} \rangle$ in much of the Cache Slough Complex during the dry season (Morgan-King & Schoellhamer, 2013).

We present two estimates of sediment trapping, one assuming only along-channel SSF and the other assuming only lateral SSF into the SAV. For the first estimate, the fraction of SSF trapped in the vegetation is

$$F = B_x \frac{u_v}{\overline{u}} \left(1 - \frac{\mathrm{SSC}_v}{\mathrm{SSC}_{zv}} \right)$$

where SSC_{zv} is channel SSC at the elevation of the SAV. Setting $B_x = 0.16$, $u_v / \overline{u} = 0.1$, and $\mathrm{SSC}_v / \mathrm{SSC}_{zv} = 0.8$ yields $F = 0.0032$. Trapping per tidal cycle is $T_1 = F\left|\mathrm{SSF}_f\right| + \left|\mathrm{SSF}_e\right|$, where SSF_f and SSF_e are cumulative $\mathrm{SSF_A}$ for the flood and ebb tide, yielding 35 kg of sediment per semidiurnal tidal cycle or 1.7% of the sediment retained in Lindsey Slough above the study transect.

The second estimate of sediment trapping in the SAV is

$$T_2 = \langle \mathrm{SSC}_{zv} \rangle \left(1 - \frac{\mathrm{SSC}_v}{\mathrm{SSC}_{zv}} \right) \Delta V_v E_f$$

where ΔV_v is the change in volume occupied by vegetation from low to high tide per m of channel length, and E_f is the flood-tide excursion. For the LS channel cross-section, ΔV_v is $32\mathrm{m}^3$ / m and E_f averages 2.62 km. Setting $\langle \mathrm{SSC}_{zv} \rangle = 9.5$mg / L (the average for 6–13 April) and $\mathrm{SSC}_v / \mathrm{SSC}_{zv} = 0.8$ yields sediment trapping

of 159 kg per semidiurnal tidal cycle or 8% of $\langle SSF_A \rangle$. T_1 and T_2 bracket the actual trapping, which results from a combination of longitudinal and lateral flux. T_1 depends on u_v / $\overline{u}$ while T_2 does not, indicating that the relative contribution of T_1 is inversely related to current attenuation in the SAV. With 90% attenuation in *E. densa*, T_2 cannot be neglected.

Lindsey Slough is depositional, and in the absence of SAV, trapping would be roughly proportional to area; so 2%–8% trapping in 16% of the channel area represents a decrease in sediment retention. The influence on the SSC, if detectable, is an increase rather than a decrease. The values of B_x and ΔV_v in LS are typical for channels, and in other deadend sloughs in the Delta T_1, T_2, and their relative contribution are likely similar to that in LS. However, in more energetic channels with little deposition and ebb-directed $\langle SSF_A \rangle$, like the Mokelumne River, trapping of 2%–8% of $\langle SSF_A \rangle$ would comprise a significant increase in the amount of stored sediment and could cause a detectable reduction of SSC in the channel.

In a related study, Work et al. (2020) estimated that SAV traps 0.025% of cumulative channel SSF. The comparable value in our study is F (0.32%). The result by Work et al. (2020) relied on instantaneous measurements of trapping and thus, like our T_1, did not account for the sediment introduced by the lateral tidal filling and draining of the vegetated margin.

Shallow tidal basins have become more common in the Delta in recent decades due to the tidal restoration of subsided agricultural tracts. Compared to channels, we expect that in shallow tidal basins u_v / $\overline{u}$ is comparable but B_x is greater, and SSC_v / SSC_{zv} is lower because SAV suppresses wind waves. As a result, F should be greater. In shallow basins ΔV_v and thus T_2 are greater than in channels, and the relative importance of T_2 is likely also greater. These factors suggest that shallow basins may account for a significant portion of vegetative sediment trapping in the Delta.

Hestir et al. (2016) hypothesized that sediment trapping by IAV is a significant factor in the SSC reduction in recent decades in the Delta. Our analysis confirms the potential for SAV to reduce SSC on a larger scale. It also highlights the potential for both the magnitude of trapping and its impact on channel SSC and $\langle SSF_A \rangle$ to vary with site-specific factors including the extent of vegetative cover and whether the setting is erosional or depositional.

4.3. Influence of *E. densa* on Sediment Flux to Local Marshes

Most Delta marshes rely on the supply of sediment from adjacent waters to maintain elevation relative to the tidal frame, and rising sea levels increase the required rate of accretion (Drexler, 2011). Because of the prevalence of *E. densa* along channel margins in the Delta, sediment transported from the channel to many marshes must pass through or over SAV. Sediment delivery to a marsh is a function of SSC in incoming waters and inundation time (Kirwan et al., 2010). While the inundation period is not influenced by fringing vegetation, *E. densa* reduces SSC by approximately 20%, so sediment supplied to marshes is decreased by 20%.

Our results also indicate that the suspended sediment carried into marshes behind SAV is entirely mud because any sand in suspension will settle out in the SAV. The floc fraction retained by SAV is likely composed of particles with relatively higher w_s, leaving a population of particles with lower w_s to inundate the marsh. This process may further decrease sediment retention on the marsh. Conversely, dissolved organic matter within SAV and over the marsh may promote flocculation, which would increase w_s and retention. These potential effects of particle size dynamics are important topics for further investigation.

Some conditions (beyond what we measured) may partially offset the 20% depletion of SSC in the SAV. Delta marshes are only inundated during high tides or high river flows, coinciding with times when *E. densa* does not reach the water surface. As discussed in Section 3.7, these conditions may allow some sediment transport above the SAV, and at more energetic sites, turbulence generated at the vegetation–water interface may resuspend sediment trapped on the vegetation. During site visits, we observed that the sediment caught on plants is easily mobilized, and minor disturbances produced clouds of high turbidity. Thus, some of the sediment trapped by SAV at lower tidal stages or low flow conditions may be mobilized at high tide or during high flows and transported onto the marsh.

SSC has declined throughout the Delta in recent decades, reducing the sediment available to marshes (Hestir et al., 2016). Thus, the reduction in SSC reaching marshes due to the presence of fringing IAV compounds the effect of the Delta-wide SSC depletion, further increasing marsh vulnerability to sea-level rise.

5. Conclusions

Egeria densa biomass density, frontal area, and areal density were similar, and currents within the SAV were strongly damped, at two sites in the Sacramento–San Joaquin Delta: A backwater slough (Lindsey Slough, LS) and a channel with stronger currents and riverine influence (Mokelumne River, MOK). Current attenuation at MOK was greater than 90% for depth-averaged channel velocities of 0.1–0.4 m/s. Bulk vegetative drag coefficient C_d was inversely related to stem Reynolds number, following $C_d = 174 Re_d^{-1.46}$, based on MOK data. This quantification of the alterations of the physical environment within SAV can advance understanding of ecological consequences of the *E. densa* invasion in the Delta, and support modeling of large-scale physical impacts wherever dense SAV occurs.

In Lindsey Slough, trapping of suspended sediment by SAV averaged 18%. The rate of vegetative trapping varied widely (0%–40%) at MOK as a function of current speed, SSC, and particle size in suspension, with greatest trapping when river discharge and SSC were elevated. Sediment accumulation rates measured in cores were greater in MOK than in LS, consistent with greater average SSC and proximity to riverine sediment sources at MOK (Drexler et al., 2021).

E. densa inhabits shallow waters and forms dense fringing canopies along many Delta channels. This spatial distribution combined with strong current attenuation focuses flow and sediment transport into the unobstructed channel. Sediment is introduced into the vegetation by both longitudinal and lateral SSF, with the importance of lateral flux increasing with current attenuation in the SAV. Sediment trapping by the SAV has the potential to reduce channel SSC, but the magnitude and sign of this effect varies with local factors including vegetative coverage and whether tidally averaged SSF is landward or seaward.

Trapping by invasive SAV significantly reduces sediment supply to Delta marshes. Water and sediment transported to marshes on each tidal cycle must pass through or over the *E. densa* on channel margins. The reduction in sediment supply to these marshes scales with the reduction in SSC (e.g., 20% in LS) in SAV. Occurring over the same timeframe as a Delta-wide decrease in SSC (Hestir et al., 2016), this decrease in sediment delivery due to invasive fringing SAV poses a significant threat to the ability of Delta marshes to maintain elevation as sea levels rise. *E. densa* is likely impacting freshwater tidal marshes worldwide in a similar manner.

Data Availability Statement

The data collected for this project are available at https://doi.org/10.5066/P9112AIP (Lacy et al., 2020).

Acknowledgments
This project involved extensive field work, made possible by the expertise of Dan Powers, Pete DalFerro, Tim Elfers, Jenny White McKee, Cordell Johnson, Andrew Stevens, and Melissa Foley. Reviews by Dan Nowacki, Dave Schoellhamer, and anonymous referees improved the manuscript. Evan Dailey prepared Figures 1 and 2. This project was funded by the U.S. Geological Survey Priority Landscapes Program for the San Francisco Bay and Delta and the U.S. Geological Survey Coastal and Marine Hazards and Resources Program. Any use of trade, firm, or product names is for descriptive purposes only and does not imply endorsement by the U.S. Government.

References

Allen, R. M., Lacy, J. R., Stacey, M. T., & Variano, E. A. (2019). Seasonal, spring-neap, and tidal variation in cohesive sediment transport parameters in estuarine shallows. *Journal of Geophysical Research*, *124*, 7265–7284. https://doi.org/10.1029/2018JC014825

Baugh, J. V., & Manning, A. J. (2007). An assessment of a new settling velocity parameterization for cohesive sediment transport modeling. *Continental Shelf Research*, *27*, 1835–1855. https://doi.org/10.1016/j.csr.2007.03.003

Bos, A. R., Bouma, T. J., de Kort, G. L., & van Katwijk, M. (2007). Ecosystem engineering by annual intertidal seagrass beds: Sediment accretion and modification. *Estuarine, Coastal and Shelf Science*, *74*, 344–348. https://doi.org/10.1016/j.ecss.2007.04.006

Chambers, P. A., Prepas, E., Hamilton, H., & Bothwell, M. (1991). Current velocity and its effect on aquatic macrophytes in flowing waters. *Ecological Applications*, *1*(3), 249–257. https://doi.org/10.2307/1941754

Cohen, A. N., & Carlton, J. T. (1998). Accelerating invasion rate in a highly invaded estuary. *Science*, *279*, 555–558. https://doi.org/10.1126/science.279.5350.555

Conomos, T. J., Smith, R. E., & Gartner, J. W. (1985). Environmental setting of San Francisco Bay. In J. E. Cloern, & F. H. Nichols (Eds.), *Temporal dynamics of an estuary: San Francisco Bay* (pp. 1–12). W. Junk Publishers. https://doi.org/10.1007/978-94-009-5528-8_1

Drexler, J. Z. (2011). Peat formation processes through the millenia in tidal marshes of the Sacramento–San Joaquin River Delta, California, USA. *Estuaries and Coasts*, *34*, 900–911. https://doi.org/10.1007/s12237-011-9393-7

Drexler, J. Z., Khanna, S., & Lacy, J. R. (2021). Carbon storage and sediment trapping by *Egeria densa* Planch., a globally invasive, freshwater macrophyte. *Science of the Total Environment*, *755*, 142602. https://doi.org/10.1016/j.scitotenv.2020.142602

Durand, J., Fleenor, W., McElreath, R., Santos, M. J., & Moyle, P. (2016). Physical controls on the distribution of the submersed aquatic weed *Egeria densa* in the Sacramento–San Joaquin delta and implications for habitat restoration. *San Francisco Estuary and Watershed Science*, *14*(1). https://doi.org/10.15447/sfews.2016v14iss1art4

Fredsoe, J., & Deigaard, R. (1992). Mechanics of Coastal Sediment Transport (Vol. 3). World Scientific.

Fregoso, T. A., Wang, R., Alteljevich, E., & Jaffe, B. E. (2017). San Francisco Bay-Delta bathymetric/topographic elevation model (DEM) (Data Release). *U.S. Geological Survey*. https://doi.org/10.5066/F7GH9G27

Gurbisz, C., Kemp, W. M., Sanford, L. P., & Orth, R. J. (2016). Mechanisms of storm-related loss and resilience in a large submersed plant bed. *Estuaries and Coasts*, *39*, 951–966. https://doi.org/10.1007/s12237-016-0074-4

Hansen, J. C., & Reidenbach, M. A. (2013). Seasonal growth and senescence of a *Zostera marina* seagrass meadow alters wave-dominated flow and sediment suspension within a coastal bay. *Estuaries and Coasts*, *36*, 1099–1114. https://doi.org/10.1007/s12237-013-9620-5

Hestir, E. L., Schoellhamer, D. H., Greenberg, J., Morgan-King, T., & Ustin, S. L. (2016). The effect of submerged aquatic vegetation expansion on a declining turbidity trend in the Sacramento–San Joaquin River Delta. *Estuaries and Coasts*, *39*, 1100–1112. https://doi.org/10.1007/s12237-015-0055-z

Jones, J. J., Collins, A. L., Naden, P. S., & Sear, D. A. (2012). The relationship between fine sediment and macrophytes in rivers. *River Research and Applications*, *38*, 1006–1018. https://doi.org/10.1002/rra.1486

Kirwan, M. L., Guntenspergen, G. R., D'Alpaos, A., Morris, J. T., Mudd, S. M., & Temmerman, S. (2010). Limits on the adaptability of coastal marshes to rising sea level. *Geophysical Research Letters*, *37*(L23401), a–n. https://doi.org/10.1029/2010GL045489

Lacy, J. R., Ferreira, J. T., Dailey, E., Dartnell, P., Drexler, J. Z., Allen, R. M., & Stevens, A. W. (2020). Sediment transport and aquatic vegetation data from three locations in the Sacramento–San Joaquin Delta, California, 2017 to 2018 (data release). *U.S. Geological Survey*. https://doi.org/10.5066/P9112AIP

Lacy, J. R., & Wyllie-Echeverria, S. (2011). The influence of current speed and vegetation density on flow structure in two macrotidal eelgrass canopies. *Limnology and Oceanography: Fluids and Environments*, *1*(1), 38–55. https://doi.org/10.1215/21573698-1152489

Lightbody, A. F., & Nepf, H. M. (2006). Prediction of velocity profiles and longitudinal dispersion in emergent salt marsh vegetation. *Limnology & Oceanography*, *51*(1), 218–228. https://doi.org/10.4319/lo.2006.51.1.0218

Lopez, F., & Garcia, M. (2001). Mean flow and turbulence structure of open-channel flow through non-emergent vegetation. *Journal of Hydraulic Engineering*, *127*(5), 392–402. https://doi.org/10.1061/(asce)0733-9429(2001)127:5(392)

Luhar, M., & Nepf, H. M. (2013). From the blade scale to the reach scale: A characterization of aquatic vegetative drag. *Advances in Water Resources*, *51*, 305–316. https://doi.org/10.1016/j.advwatres.2012.02.002

Luoma, S. N., Dahn, C. N., Healey, M., & Moore, J. N. (2015). Challenges facing the Sacramento–San Joaquin Delta: Complex, chaotic, or simply cantankerous? *San Francisco Estuary and Watershed Science*, *13*(3). https://doi.org/10.15447/sfews.2015v13iss3art7

Madsen, J., Chambers, P., James, W., Koch, E., & Westlake, D. (2001). The interaction between water movement, sediment dynamics and submersed macrophytes. *Hydrobiologia*, *444*, 71–84. https://doi.org/10.1023/a:1017520800568

Manning, A. J., & Schoellhamer, D. H. (2013). Factors controlling floc settling velocity along a longitudinal estuarine transect. *Marine Geology*, *145*, 266–280. https://doi.org/10.1016/j.margeo.2013.06.018

Mikkelsen, O. A., & Pejrup, M. (2001). The use of a LISST-100 laser particle sizer for in-situ estimates of floc size, density and setling velocity. *Geo-Marine Letters*, *20*, 187–195. https://doi.org/10.1007/s003670100064

Morgan-King, T., & Schoellhamer, D. H. (2013). Suspended-sediment flux and retention in a backwater tidal slough complex near the landward boundary of an estuary. *Estuaries and Coasts*, *36*, 300–318. https://doi.org/10.1007/s12237-012-9574-z

Nepf, H. M. (2012). Hydrodynamics of vegetated channels. *Journal of Hydraulic Research*, *50*(3), 262–279. https://doi.org/10.1080/00221686.2012.696559

Nepf, H. M., & Vivoni, E. (2000). Flow structure in depth-limited, vegetated flow. *Journal of Geophysical Research*, *105*, 28. https://doi.org/10.1029/2000jc900145

Nichols, F. H., Cloern, J. E., Luoma, S. N., & Peterson, D. H. (1986). The modification of an estuary. *Science*, *231*(4738), 567–573. https://doi.org/10.1126/science.231.4738.567

Nobriga, M. L., Feyrer, F., Baxter, R. D., & Chotkowski, M. (2005). Fish community ecology in an altered river delta: Spatial patterns in species composition, life history strategies, and biomass. *Estuaries*, *28*(5), 776–785. https://doi.org/10.1007/BF02732915

Santos, M. J., Anderson, L. W., & Ustin, S. L. (2011). Effects of invasive species on plant communities: An example using submersed aquatic plants at the regional scale. *Biological Invasions*, *13*, 443–457. https://doi.org/10.1007/s10530-010-9840-6

Siegel, A. F. (1982). Robust regression using repeated medians. *Biometrika*, *69*(1), 242–244. https://doi.org/10.1093/biomet/69.1.242

Singh, D., Ting, M., Scaife, A. A., & Martin, N. (2018). California winter precipitation predictability: Insights from the anomolous 2015–2016 and 2016–2017 seasons. *Geophysical Research Letters*, *45*(L23617), 9972–9980. https://doi.org/10.1029/2018GL078844

Sommer, T., Armor, C., Baxter, R., Breuer, R., Brown, L., Chotkowski, M., et al. (2007). The collapse of pelagic fishes in the upper San Francisco Estuary. *Fisheries*, *32*(6), 270–277. https://doi.org/10.1577/1548-8446(2007)32[270:tcopfi]2.0.co;2

Sukhodolova, T. A., & Sukhodolov, A. N. (2012). Vegetated mixing layer around a finite-size patch of submerged plants: 1. Theory and field experiments. *Water Resources Research*, *48*(W10533). https://doi.org/10.1029/2011WR011804

Swanson, K. M., Drexler, J. Z., Fuller, C. C., & Schoellhamer, D. H. (2015). Modeling tidal freshwater marsh sustainability in the Sacramento–San Joaquin delta under a broad suite of potential future scenarions. *San Francisco Estuary and Watershed Science*, *13*(1). https://doi.org/10.15447/sfews.2015v13iss1art3

Tanino, Y., & Nepf, H. (2008). Laboratory investigation of mean drag in a random array of rigid, emergent cylinders. *Journal of Hydraulic Engineering*, *134*(1). https://doi.org/10.1061/10.1061/(asce)0733-9429(2008)134:1(34)

van Katwijk, M., Bos, A., Hermus, D. R., & Suykerbuyk, W. (2010). Sediment modification by seagrass beds: Muddification and sandification induced by plant cover and environmental conditions. *Estuarine, Coastal and Shelf Science*, *89*(2), 175–181. https://doi.org/10.1016/j.ecss.2010.06.008

Vargas-Luna, A., Crosato, A., & Uijttewaal, W. S. (2015). Effects of vegetation on flow and sediment transport: Comparative analyses and validation of predicting models. *Earth Surface Processes and Landforms*, *40*, 157–176. https://doi.org/10.1002/esp.3633

Winterwerp, J. C. (1998). A simple model for turbulence induced flocculation of cohesive sediment. *Journal of Hydraulic Research*, *36*(3), 309–326. https://doi.org/10.1080/00221689809498621

Work, P. A., Downing-Kunz, M., & Drexler, J. Z. (2020). Trapping of suspended sediment by submerged aquatic vegetation in a tidal freshwater region: Field observations and long-term trends. *Estuaries and Coasts*, *44*, 734–749. https://doi.org/10.1007/s12237-020-00799-w

Wright, S. A., Schoellhamer, D. H., (2004). Trends in the sediment yield of the Sacramento River, California, 1957-2001. *San Francisco Estuary and Watershed Science*, *2*(2), https://doi.org/10.15447/sfews.2004v2iss2art2

Wright, S. A., & Schoellhamer, D. H. (2005). Estimating sediment budgets at the interface between rivers and estuaries with application to the Sacramento–San Joaquin River Delta. *Water Resources Research*, *41*. https://doi.org/10.1029/2004WR003725

Yarrow, M., Marín, V. H., Finlayson, M., Tironi, A., Delgado, L. E., & Fischer, F. (2009). The ecology of *Egeria densa* planchon (Liliopsida: Alismatales): A wetland ecosystem engineer? *Revista Chilena de Historia Natural*, *82*, 299–313. https://doi.org/10.4067/s0716-078x2009000200010